J. U. ANDERSEN

AXIAL AND PLANAR DIPS IN REACTION YIELD FOR ENERGETIC IONS IN CRYSTAL LATTICE

Det Kongelige Danske Videnskabernes Selskab
Matematisk-fysiske Meddelelser **36**, 7

Kommissionær: Munksgaard
København 1967

CONTENTS

Synopsis

Computer programs have been developed to calculate numerically the dips in yield along low-index directions and planes of energetic positively charged particles emitted isotropically from substitutional sites in a crystal lattice. The calculations are based on Lindhard's theoretical treatment of directional effects and include effects of thermal vibrations of the emitting atoms. The obtained intensity distributions also give the nuclear reaction yield as a function of the direction of an incident beam.

PRINTED IN DENMARK
BIANCO LUNOS BOGTRYKKERI A/S

Introduction

During the last few years, directional effects connected with the passage of swift charged particles through a crystal lattice have been studied intensively in a number of laboratories, both experimentally and theoretically. Perhaps the most interesting effect observed is the almost complete extinction of nuclear reactions for positively charged particles incident on a single crystal parallel to a low-index direction[1] or plane[2]. This shadow phenomenon has already been shown to be a very useful tool in solid state investigations[3]. The present work contains numerical evaluations of some of the related formulas derived in the comprehensive theoretical treatment[4]* given by LINDHARD. Although the main purpose is to give quantitative theoretical estimates, the results of the numerical calculations may also serve as an illustration of the fundamental qualitative aspects of Lindhard's theoretical treatment.

The calculations to be presented in the following are directly concerned with the emission of positively charged particles from lattice sites. The obtained probability distributions for the direction of emergence of the particles from the crystal, however, also give the probability for particles incident on the crystal to hit a lattice atom as a function of the direction of incidence. This may easily be verified by direct calculation, but may also be regarded as a consequence of the reversibility rule discussed in I, § 5.

The first two paragraphs contain the formulas on which the calculations are based. The reader is referred to I for derivation and further discussion of these formulas.

§ 1. Emission of Particles from a String

The basic approximation in I is that of an isolated string of atoms, i.e. the interaction of a particle moving at a small angle to a low-index direction is treated as the interaction of the particle with isolated strings or rows of atoms. This simplifies very much the theoretical description. Furthermore,

* In the following referred to as I.

it is shown in I that this interaction may be treated essentially by classical mechanics*.

As a first approximation (the continuum approximation), the atomic potentials are replaced by an average potential $U(r)$ given by

$$U(r) = \int_{-\infty}^{\infty} \frac{dz}{d} V\left(\sqrt{r^2 + z^2}\right), \tag{1}$$

where r is the distance from the string, $V(R)$ the atomic potential, and d the distance between atoms in the string. In this approximation, the transverse energy of a particle $E_\perp = E\varphi^2 + U(r)$ is conserved in a collision with a string.

In I, Appendix A, this description is refined by considering the transverse energy at the planes perpendicular to the string half-way between atoms. It is shown in a direct way that the transverse energy defined in this way is approximately conserved when the angle between the particle path and the string is small.

On the basis of this approximation, the emission of a particle from a string atom is considered in I, § 6. The particle motion is divided into three stages:

a) Emission from the string atom
b) Passage through the crystal lattice
c) Transmission through the crystal surface.

Figure 1 illustrates the calculation of the distribution in transverse energy after stage a). The particle A with energy E is emitted from atom B. The angle of emission is φ and ϑ is the azimuthal angle of emission. At the moment of emission, the atom is at a distance r from an otherwise perfect string. Thus, the thermal vibrations of all string atoms except the emitting atom are neglected, whereas the thermal vibrations of the emitting atom are represented by a probability distribution for r, $dP(r)$, which is taken as a Gaussian:

$$dP(r) = e^{-r^2/\varrho^2} \frac{d(r^2)}{\varrho^2} \cdot \alpha, \tag{2}$$

where $\alpha \simeq 1$ is a normalization constant and ϱ^2 the mean square displacement perpendicular to the string.

* For a general quantum mechanical treatment, the reader is referred to ref. 5).

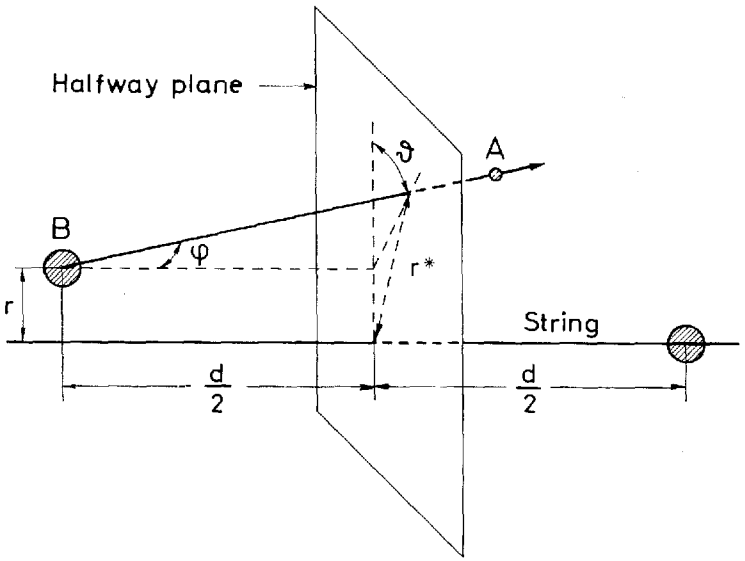

$$E_\perp = E\varphi^2 + U(r^*)$$

$$r^{*2} = r^2 + \left(\frac{\varphi d}{2}\right)^2 + r\varphi d \cos\vartheta$$

Fig. 1. Emission of particle from string atom.

The emission is assumed to be isotropic. Consequently, the probability distribution for φ is proportional to φ (for small angles φ) and for ϑ a constant. The transverse energy of the emitted particle is calculated at the half-way plane as the sum of the transverse kinetic energy $E\varphi^2$, and the transverse potential energy $U(r^*)$.

From this, an expression for the distribution in transverse energy after stage a) is derived*:

$$\Pi_{\text{out}}(E_\perp) = \int_{r=0}^{r_0} dP(r) \int d(E\varphi^2) \int_0^{2\pi} \frac{d\vartheta}{2\pi} \cdot \delta(E_\perp - U(r^*) - E\varphi^2). \tag{3}$$

Here, r_0 is given by $\pi r_0^2 = (Nd)^{-1}$, where N is the number of atoms per cm^3 and d the distance between the atoms on the string. The other parameters are indicated in Fig. 1.

* Here, and in the following, the probability distributions are normalized to the random case, i.e. to $U(r) \equiv 0$.

According to I, Appendix A, the transverse energy of the particle is not changed by collisions with perfect strings. In the following, we neglect the change in transverse energy during stage b) of the motion caused by thermal vibrations of the atoms on the strings and assume strict conservation of transverse energy in stage b).

Stage c) of the particle motion is the transmission through the crystal surface. The transverse energy $E\psi_e^2$ of a particle, which has been transmitted through the crystal surface at a distance r from a string, is given by $E\psi_e^2 = E_\perp - U(r)$, where $E_\perp$ is the transverse energy before the transmission. Consequently, the distribution in transverse energy outside the crystal surface $P_e(E\psi_e^2)$ becomes

$$P_e(E\psi_e^2) = \int dE_\perp \Pi_{\text{out}}(E_\perp) T(E\psi_e^2, E_\perp), \tag{4}$$

where the transmission factor $T(E\psi_e^2, E_\perp)$ is given by

$$T(E\psi_e^2, E_\perp) = \int_0^{r_0} \frac{d(r^2)}{r_0^2 - \hat{r}^2(E_\perp)} \delta\big(E_\perp - E\psi_e^2 - U(r)\big). \tag{5}$$

Here, $\hat{r}(E_\perp)$ is defined by $U\big(\hat{r}(E_\perp)\big) = E_\perp$.

The transmission factor $T(E\psi_e^2, E_\perp)$ is analogous to I, eq. (6.1), the transmission factor for particles incident on a crystal surface. The only difference is that r_0^2 in the denominator is replaced by $r_0^2 - \hat{r}^2(E_\perp)$ because the particle motion is restricted to that part of the transverse plane where $E_\perp > U(r)$.

From (4) and (5) we get

$$P_e(E\psi_e^2) = \int_0^{r_0} \frac{d(r^2)}{r_0^2 - \hat{r}^2\big(E\psi_e^2 + U(r)\big)} \Pi_{\text{out}}\big(E\psi_e^2 + U(r)\big). \tag{6}$$

Formula (3) is in I treated analytically in the continuum approximation: $r^* = r$, and an explicit expression for $\Pi_{\text{out}}(E_\perp)$ is derived, using the standard potential I, eq. (2.6):

$$U(r) = \tfrac{1}{2} E\psi_1^2 \cdot \log\left(\left(\frac{Ca}{r}\right)^2 + 1\right), \tag{7}$$

where

$$\psi_1 = \left(\frac{2Z_1 Z_2 e^2}{d \cdot E}\right)^{1/2};$$

a is the Thomas-Fermi screening radius and $C \simeq \sqrt{3}$. The result is

$$\Pi_{\text{out}}(E_\perp) = \exp\left\{-\frac{C^2a^2}{\varrho^2}\left(e^{\frac{2E_\perp}{E\psi_1^2}}-1\right)^{-1}\right\} - \exp\left\{-\frac{r_0^2}{\varrho^2}\right\}. \tag{8}$$

Furthermore, a qualitative estimate, I, eq. (6.12), of the integrated dip is given:

$$\Omega \simeq \pi \cdot \frac{\psi_1^2}{2} \cdot \log\frac{\gamma C^2a^2+\varrho^2}{\varrho^2}, \tag{9}$$

where $\gamma = 1.78$ is Euler's constant.

Except at low energies, where $\psi_1 \gtrsim a/d$, formula (8) gives a good approximation for the width of the dip and its dependence on the vibrational amplitude ϱ. The important feature of compensation, however, is missing in this continuum description. The accuracy of the formulas (8) and (9) is further discussed in § 5.

§ 2. Emission of Particles from a Plane

A similar, but weaker correlation of successive small angle scattering events exists for a particle moving at a small angle to a low-index crystal plane. The scattering of the particle by a plane of atoms may, as a first approximation, be treated as the motion in an average planar potential:

$$Y(y) = N \cdot d_p \int_0^\infty 2\pi r dr\; V\left(\sqrt{y^2+r^2}\right), \tag{10}$$

where $N \cdot d_p$ represents the atomic density in the plane, N being the number of atoms per cm^3 and d_p the distance between planes. In this approximation, the transverse energy $E_\perp = E\varphi^2 + Y(y)$ of a particle with respect to a plane is conserved.

In the string case, the continuum description was improved by measuring the transverse energy at the half-way planes. A similar refinement is not straightforward in the planar case because of the less well-defined correlation between successive scattering events. The need for such a refinement is, however, smaller in the planar case since the planar potential decreases more slowly with distance than the string potential, and the critical angles for planes are smaller. Furthermore, the compensation of the dip is already contained in the continuum description of the planar case as may easily

be seen by integrating formula (12) with respect to $E_\perp$. Consequently, in the following, the planar case is treated in the continuum approximation.

Formulas for the distribution in transverse energy of particles emitted from a planar atom are not given explicitly in I but may easily be derived in analogy to the string case. Again, zero-point and temperature vibrations are represented by a Gaussian distribution of the distance y of the emitting atom from the plane at the moment of emission:

$$dP(y) = \frac{2}{\sqrt{\pi}} e^{-y^2/\varrho^2} dy \frac{\alpha}{\varrho}, \tag{11}$$

where α is a normalization constant, $\alpha \simeq 1$, and ϱ^2 is the mean square displacement perpendicular to the plane. If the emission is assumed to be isotropic, the probability distribution for the angle of emission φ is a constant (for small angles φ).

The transverse $E_\perp$ of the emitted particle is the sum of the transverse kinetic energy $E\varphi^2$, where E is the energy of the emitted particle, and the transverse potential energy $Y(y)$. Thus, the distribution in transverse energy $\Pi_{\text{out}}(E_\perp)$ after stage a) becomes

$$\left.\begin{aligned} \Pi_{\text{out}}(E_\perp) &= \int_0^{d_p/2} dP(y) \int d(E\varphi^2) \left(\frac{E_\perp}{E\varphi^2}\right)^{1/2} \delta\left(E_\perp - E\varphi^2 - Y(y)\right) \\ &= \int_{\hat{y}(E_\perp)}^{d_p/2} dP(y) \left(\frac{E_\perp}{E_\perp - Y(y)}\right)^{1/2}, \end{aligned}\right\} \tag{12}$$

where $\hat{y}(E_\perp)$ is given by $Y(\hat{y}(E_\perp)) = E_\perp$ for $E_\perp < Y(0)$ and $\hat{y}(E_\perp) = 0$ for $E_\perp > Y(0)$.

Again, we neglect the redistribution in transverse energy in stage b) and only consider stage c), the transmission through the crystal surface. This is complicated by the fact that in statistical equilibrium, the probability distribution $P_0(E_\perp, y)$ for the distance y of a particle with given transverse energy $E_\perp$ from a plane is not constant as in the two-dimensional string case, but inversely proportional to the square root of the transverse kinetic energy (I, eq. (3.2)):

$$P_0(E_\perp, y) = \begin{cases} \dfrac{K}{d_p} \cdot \left(\dfrac{E_\perp}{E_\perp - Y(y)}\right)^{1/2} & \text{for } E_\perp > Y(y) \\ 0 & \text{for } E_\perp < Y(y) \end{cases}, \tag{13}$$

where K is a normalization constant, $K = K(E_\perp)$, given by

$$K(E_\perp) = \left(\int_{\hat{y}}^{d_p/2} \frac{dy}{d_p} \left(\frac{E_\perp}{E_\perp - Y(y)}\right)^{1/2} \right)^{-1}. \tag{14}$$

The transmission factor $T(E\psi_e^2, E_\perp)$ thus becomes:

$$\begin{aligned} T(E\psi_e^2, E_\perp) &= \int_0^{d_p/2} dy\, P_0(E_\perp, y)\delta(E_\perp - E\psi_e^2 - Y(y)) \\ &= K \cdot \int_{\hat{y}(E_\perp)}^{d_p/2} \frac{dy}{d_p} \left(\frac{E_\perp}{E_\perp - Y(y)}\right)^{1/2} \delta\big(E_\perp - E\psi_e^2 - Y(y)\big). \end{aligned} \tag{15}$$

From this we get the distribution in transverse energy outside the crystal:

$$\begin{aligned} P_e(E\psi_e^2) &= \int dE_\perp \Pi_{\text{out}}(E_\perp) T(E\psi_e^2, E_\perp) \\ &= \int_0^{d_p/2} \frac{dy}{d_p} K\big(E\psi_e^2 + Y(y)\big) \cdot \left(\frac{E\psi_e^2 + Y(y)}{E\psi_e^2}\right)^{1/2} \Pi_{\text{out}}\big(E\psi_e^2 + Y(y)\big). \end{aligned} \tag{16}$$

§ 3. Thermal Vibrations

In the above formula, an Einstein model of independently vibrating lattice atoms is assumed. Furthermore, the vibrations of all atoms except the emitting atom are neglected. This may be a reasonable first approximation since the vibrations of the other atoms are averaged out when many atoms contribute to the scattering.

The mean square amplitude $\langle R^2 \rangle$ may be estimated from the Debye model (see e.g. ref. 6)):

$$\langle R^2 \rangle = \frac{9\hbar^2}{M\varkappa T_D} \left\{ \frac{1}{4} + \frac{1}{X_D} \Phi(X_D) \right\}, \tag{17}$$

where M is the atomic mass of the crystal atoms, $\varkappa$ is Boltzmann's constant, T_D the Debye temperature, and X_D defined by $X_D = T_D/T$. The function $\Phi(X_D)$ is defined by

$$\Phi(X_D) = \frac{1}{X_D}\int_0^{X_D} \frac{x\,dx}{e^x - 1}. \tag{18}$$

Φ is tabulated in e.g. ref. 7).

From (17), $\langle R^2\rangle$ may be calculated as a function of the absolute temperature T. For $T < T_D$, the term 1/4 from zero-point vibrations dominates, and for $T > T_D$, $\langle R^2\rangle$ is proportional to T.

For the mean square vibration perpendicular to a string or a plane, we have $\langle r^2\rangle = 2/3\langle R^2\rangle$ and $\langle y^2\rangle = 1/3\langle R^2\rangle$, respectively. From these relations, and from (17), the parameter ϱ in formulas (2) and (11) may be estimated.

Since the nearest neighbour plays a dominating part in the interaction of the emitted particle with the string or plane, it may be of interest to estimate the correlation between the vibrations of neighbouring atoms. This may be done[8] on the basis of a formalism as developed in ref. 6). If $u_\alpha(\vec{r})$ is the α-component of the displacement operator at the position $\vec{r}$, a correlation coefficient β for the α-components of the vibrations of the neighbouring atoms is defined by:

$$\beta = \frac{\langle u_\alpha(\vec{r})u_\alpha(\vec{r}+\vec{d})\rangle}{\langle u_\alpha(\vec{r})^2\rangle}, \tag{19}$$

where $\vec{d}$ is the distance vector between the two neighbouring atoms. As usual, $\langle\ \rangle$ denotes the expectation value.

In ref. 8), this correlation coefficient is estimated in two limits: $T \ll T_D$ and $T \gg T_D$, in the Debye approximation:

$$T \ll T_D\colon\ \beta \simeq 2\big(1 - \cos(k_D \cdot d)\big)/(k_D \cdot d)^2 \tag{20}$$

$$T \gg T_D\colon\ \beta \simeq \frac{\pi}{2} \cdot (k_D \cdot d)^{-1} \tag{21}$$

Here, k_D is defined by $k_D = (6\pi^2/V_0)^{1/3}$, where V_0 is the volume of the unit cell.

If we set $d = V_0^{1/3}$ and disregard the cosine term in (20), we get in the two limits $\beta \simeq 0.13$ and $\beta \simeq 0.40$, respectively. It is seen that, despite the correlation, the mean square relative displacement in both limits is larger than the mean square absolute displacement. In consequence, it seems justified to neglect the correlation in the present approximation.

§ 4. Numerical Calculations

String case

The intensity distribution (6) is calculated by simulating emission of particles from a vibrating string atom. First, the intensity distribution (3) is calculated. The three parameters (cf. Fig. 1), r, ϑ, and φ are varied independently in steps: $r : (1-25) \cdot \varrho/10$, $\vartheta : (1-10) \cdot \pi/10$, $\varphi : (1-50) \cdot \psi_1/10$. For each set of parameter values, the transverse energy $E_\perp$ of the particle is calculated from the relation $E_\perp = E\varphi^2 + U(r^*)$. (Lindhard's standard potential (7) has been applied with $C = \sqrt{3}$). Thereby, the emission angle ψ is determined through the relation $E\psi^2 = E_\perp$, and ψ is approximated by an integral multiple of $\psi_1/10$. The emission spectrum is obtained, each event being weighted by a factor $2\varphi \cdot r/\varrho \cdot \exp\{-r^2/\varrho^2\}$, which accounts for the probability distribution of the parameters r, ϑ, and φ.

In the last part of the program, the change in the angular distribution in stage c) – the transmission through the surface – is calculated from (6). For simplicity, $r_0^2 - \hat{r}^2$ has been replaced by r_0^2 in the program. This introduces an error of at most a few per cent for some values of the emission angle. The angle of emergence ψ_e is also approximated by an integral multiple of $\psi_1/10$.

The program contains four external parameters: $P1 = Ca/d$, $P2 = \varrho/d$, $P3 = \psi_1$, and $P4 = \pi r_0^2/d^2$. The last parameter only influences the second part of the calculation, transmission through the surface. Furthermore, the intensity distribution before this transmission has an important similarity property. As a function of ψ/ψ_1, the distribution only depends on the two parameters $P1/P2 = Ca/\varrho$ and $P2/P3 = \varrho/d\psi_1$. This may be compared to the probability distribution (8) obtained in the continuum approximation. This distribution depends only on one parameter, Ca/ϱ.

The program has been used at the GIER computer at the University of Aarhus. For one set of external parameters, the calculation takes ~5 minutes.

Planar case

In this case, the integrals in (12), (14), and (16) are calculated directly. The potential used is the continuum planar potential obtained by introducing Lindhard's standard potential I, eq. (2.6'') in (10):

$$Y(y) = 2\pi Z_1 Z_2 e^2 N d_p \left[(y^2 + C^2a^2)^{1/2} - y\right] \tag{22}$$

with $C = \sqrt{3}$.

It would have been more correct to use a potential

$$\hat{Y}(y) = Y(y) + Y(d_p - y). \tag{23}$$

However, the two potentials only differ appreciably for $y \approx d_p/2$, and the correction will therefore be of minor importance.

If a distance d is introduced by

$$N \cdot d_p \cdot d^2 = 1 \tag{24}$$

and an angle ψ_p by

$$\psi_p = \left(\frac{2Z_1Z_2e^2}{d \cdot E}\right)^{1/2} \cdot \sqrt{\frac{Ca}{d}}, \tag{25}$$

(22) is transformed into

$$Y(y) = \pi \cdot E \cdot \psi_p^2 \cdot \left[\left(\frac{y^2}{(Ca)^2} + 1\right) - \frac{y}{Ca}\right]. \tag{26}$$

It is easily seen from formulas (24), (25), (26) and from (10), (12), (14), and (16) that the shape of the intensity distribution only depends on two parameters: $p1 = Ca/\varrho$ and $p2 = Ca/d_p$. For fixed values of these two parameters, the planar dips are similar with scaling factor ψ_p. Essentially, the parameter $p2$ only influences the surface transmission so that, analogously to the continuum description of the string case (8), the intensity distribution as a function of ψ/ψ_p before transmission through the surface only depends on one parameter Ca/ϱ.

This program has also been used at the GIER computer at the University of Aarhus. For one set of parameter values, the calculation takes ~ 10 minutes.

§ 5. Results of the Numerical Calculations

String case

As mentioned above, the string dip is essentially determined by the relative magnitude of the three parameters, $P1$, $P2$, and $P3$. The influence of the fourth parameter, $P4 = \pi r_0^2/d^2$ is illustrated in Fig. 2, which shows how the transmission through the surface of the crystal changes the angular distribution. It is seen that the transmission almost exclusively influences the intensity at the bottom of the dip.

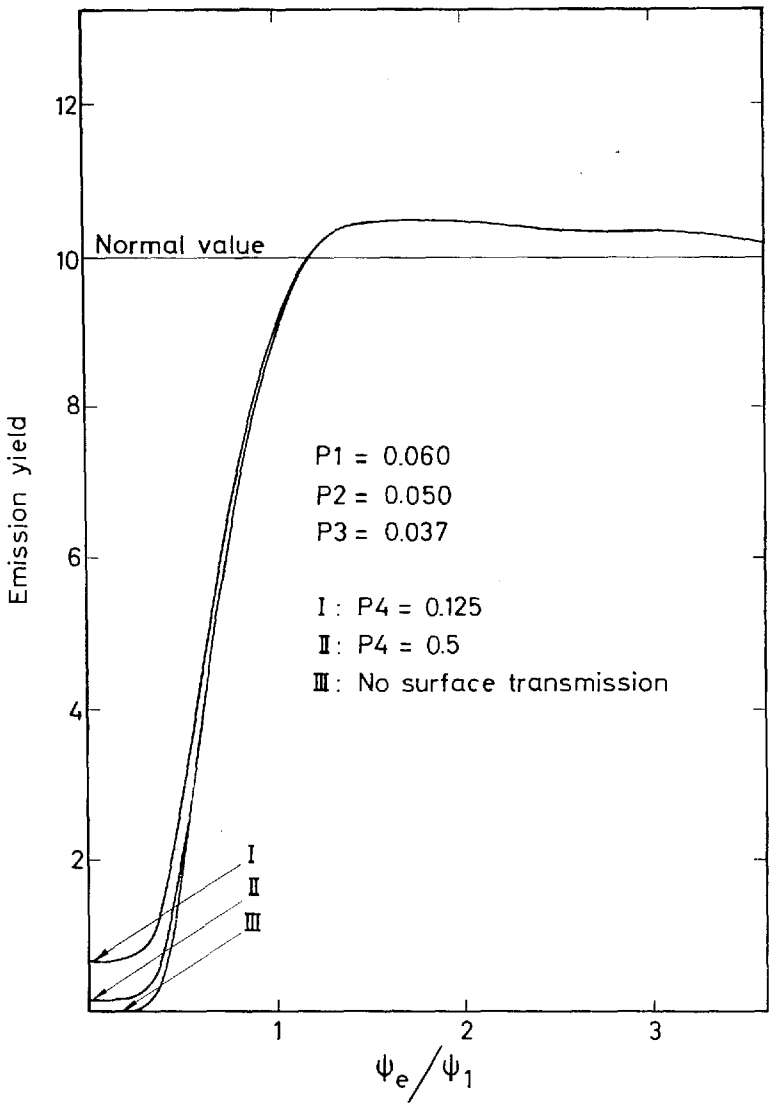

Fig. 2. Influence of the surface transmission on the angular distribution illustrated by the emission of 500 keV protons from a ⟨100⟩ string in tungsten at 1470° K. Actual value of $P4$ is 0.5.

The most important parameter is $P3 = \psi_1$. In the continuum approximation (8), angular distributions for different values of ψ_1 are similar, with scaling factor ψ_1. In the present calculation, the similarity is broken. This

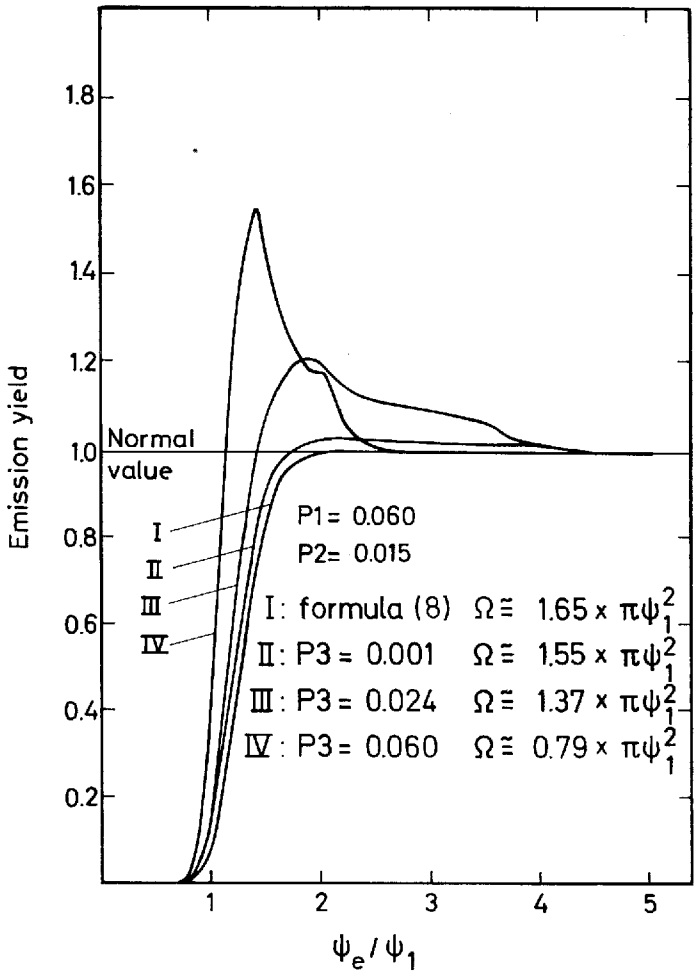

Fig. 3. Illustration of the deviations from similarity of angular distributions for varying $P3 = \psi_1$. Values of $P1$ and $P2$ correspond to emission of protons from a $\langle 100 \rangle$ string in tungsten at $\sim 100°$ K. Values II, III, and IV of ψ_1 correspond to proton energies of 700 MeV, 1.2 MeV, and 0.2 MeV, respectively. Ω is the integrated (two-dimensional) dip.

is illustrated in Fig. 3, which shows angular distribution before surface transmission for fixed values of $P1 = Ca/d$ and $P2 = \varrho/d$ and varying $P3$. Also shown in the figure is the curve calculated from (8). It is seen that the numerically calculated curves approach this curve for $P3 \to 0$. In order to compare with the approximation (9) for the integrated dip Ω, this has been calculated for each curve.

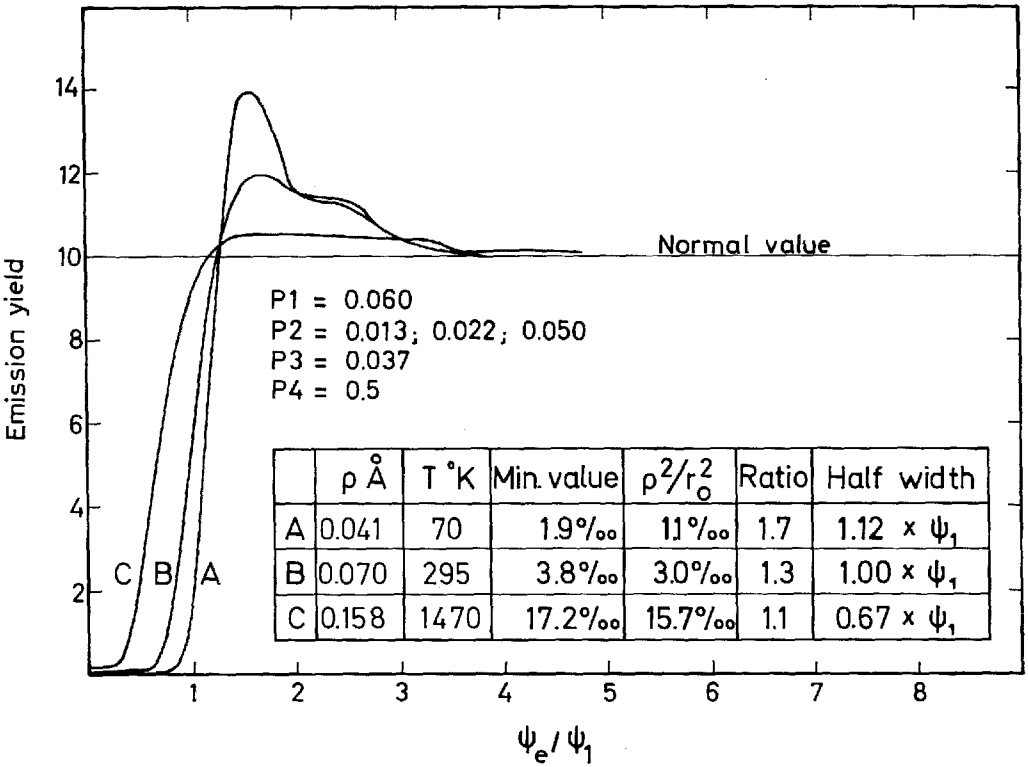

	ρ Å	T °K	Min. value	ρ^2/r_0^2	Ratio	Half width
A	0.041	70	1.9‰	1.1‰	1.7	1.12 × ψ_1
B	0.070	295	3.8‰	3.0‰	1.3	1.00 × ψ_1
C	0.158	1470	17.2‰	15.7‰	1.1	0.67 × ψ_1

Fig. 4. Influence of vibrational amplitude ϱ on angular distribution of 500 keV protons emitted from a ⟨100⟩ string in tungsten at different temperatures.

Figure 4 shows how the calculated string dips depend on $P2 = \varrho/d$. The parameters $P1$, $P3$, and $P4$ correspond to 500 keV protons incident on a tungsten crystal along a ⟨100⟩ direction. The first column in the table in the figure shows the ϱ-values, and the second column the temperatures which, in this case, correspond to the values of the parameter $P2$. The ϱ-dependence of the minimum yield is shown in the third column and compared with the value ϱ^2/r_0^2, which is the minimum yield calculated in the continuum approximation (I, eq. (6.13)). As expected, the agreement is best for large values of ϱ. The last column in the table shows the variation with ϱ of the width at half minimum of the dip.

Figures 3 and 4 also illustrate the compensation of the dip by an increase in yield at angles slightly larger than the width. The compensation is analogous to the compensation of the classical Rutherford shadow behind an atom

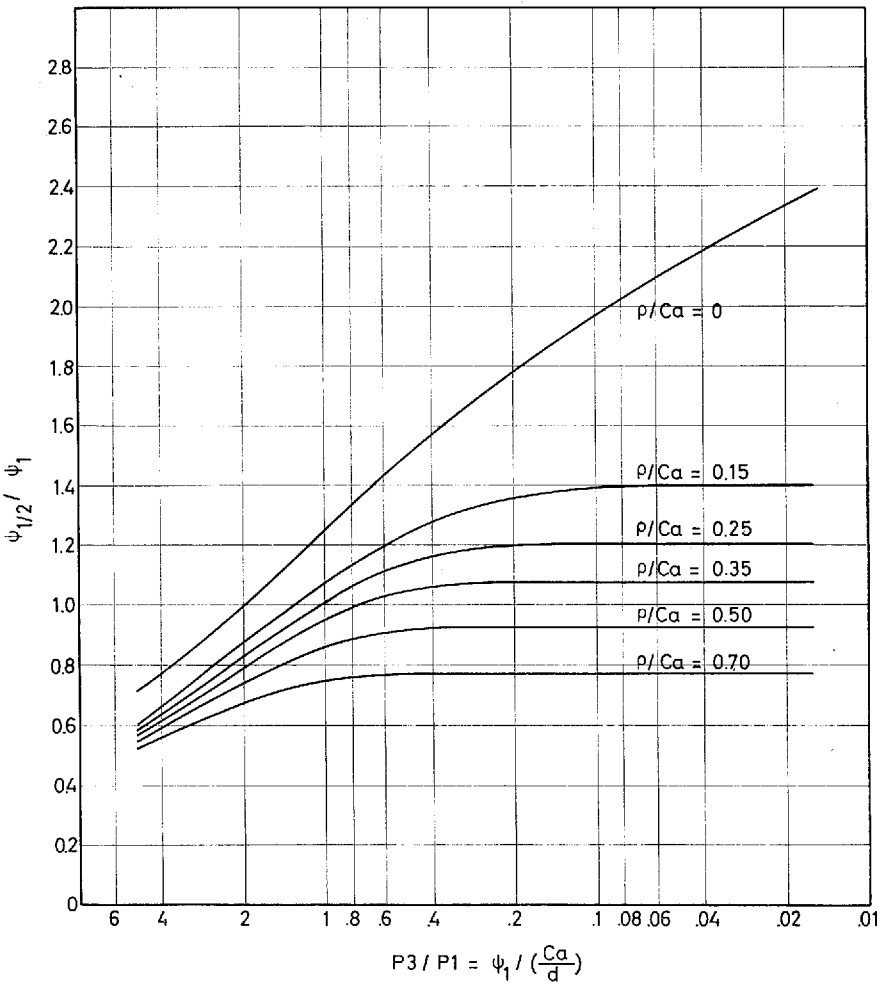

Fig. 5. Semi-logarithmic plot of the calculated half width $\psi_{1/2}$ as a function of the two parameters $\psi_1/(Ca/d)$ and ϱ/Ca.

(treated in I, § 2). In that case, half the compensation is found at angles $\sim Ca/d$. This feature is easily recognized in Figs. 3 and 4. Another qualitative feature of the compensation is seen. The high and narrow compensating shoulder found at small values of ϱ is rapidly smeared out when ϱ increases relative to $\psi_1 \cdot d$.

An important parameter, which may be extracted from the calculated curves, is the width at half dip as a function of the relative magnitude of

the three parameters $P1 = Ca/d$, $P2 = \varrho/d$, and $P3 = \psi_1$. In most cases, the surface transmission does not influence the half width very much (cf. Fig. 2). It was therefore not included in the calculations on which Fig. 5 is based. The results are plotted as a family of curves, each characterized by a fixed value of $P1/P2 = \varrho/Ca$. The curves give the half width $\psi_{1/2}$ in units of ψ_1 as a function of $P3/P1 = d\psi_1/Ca$. This family of curves is compared to the curve obtained from I, eq. (A. 19), corresponding to $\varrho = 0$. It is interesting to note that for $\psi_1 < Ca/d$, the ratio $\psi_{1/2}/\psi_1$ is almost constant and close to unity when thermal vibrations are included. As a rule of thumb, the full width at half dip may be taken to be $2\psi_1$ for $\psi_1 \lesssim Ca/d$.

The region $\psi_1 \gg Ca/d$ has not been investigated in detail, mainly because few experiments are performed at very low energies. The calculations may, however, easily be extended to cover this region.

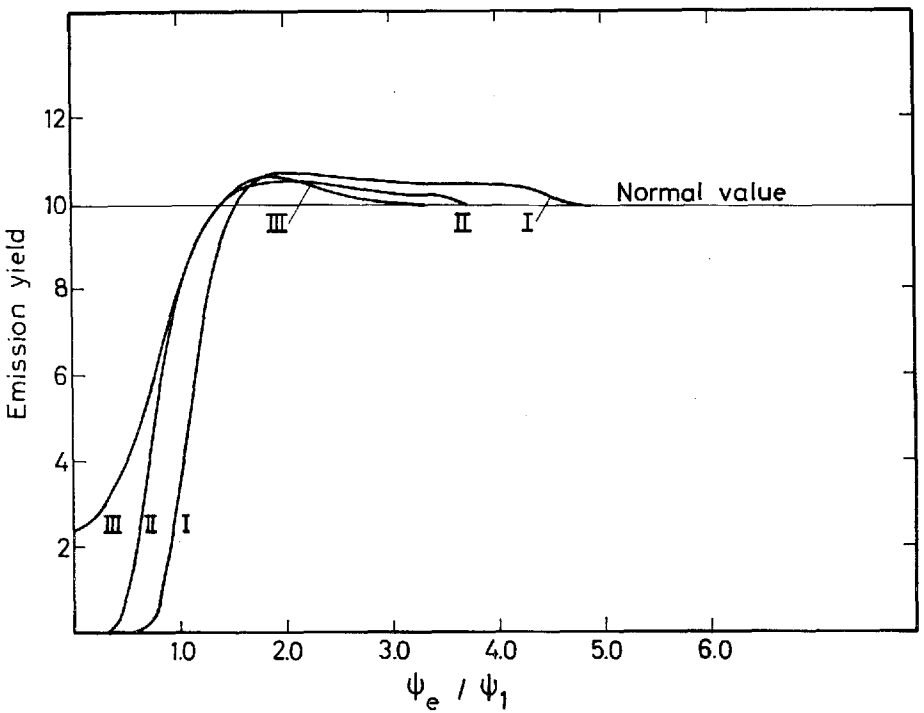

Fig. 6. Comparison of different calculations of the angular distribution of 5.49 MeV alpha particles emitted from a ⟨111⟩ string in tungsten. Curves I and II are calculated numerically with Lindhard's standard potential and a Bohr potential, respectively. Curve III is calculated by OEN[9] on the basis of a two-particle model. In all calculations, the value $\varrho = 0.054$ A has been used.

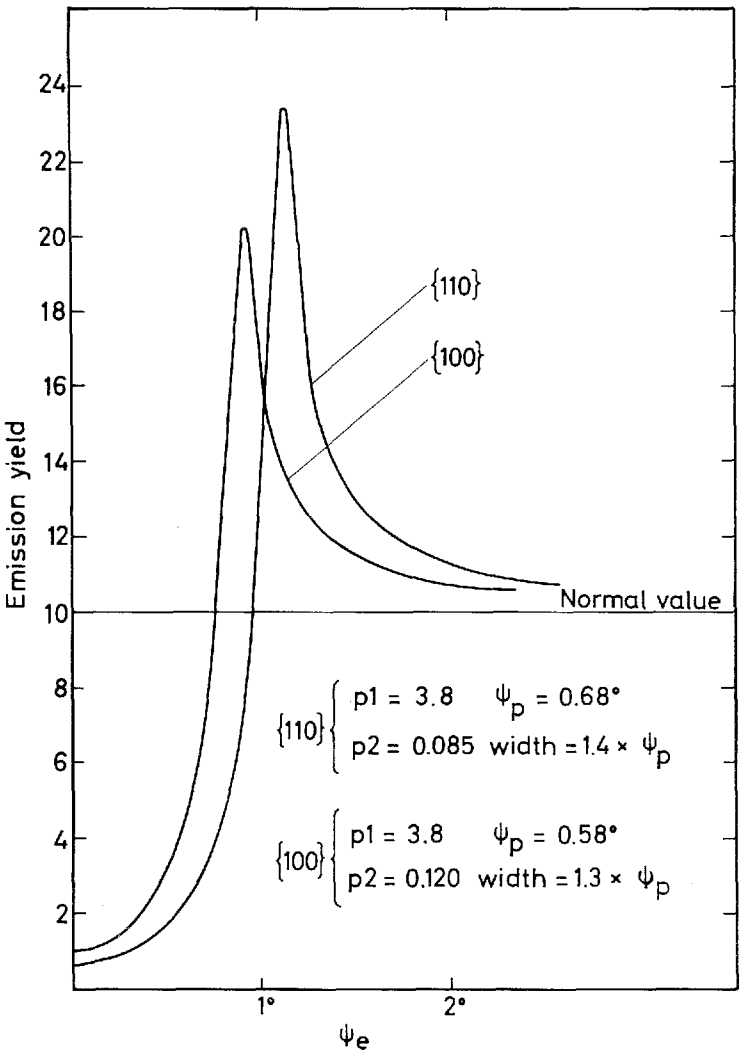

Fig. 7. Angular distribution of 400 keV protons emitted from {100} and {110} planes in tungsten at room temperature.

Comparison with numerical calculations on the basis of a two-particle model

The influence of thermal vibrations on the classical shadow behind an atom has been numerically evaluated by OEN[9]. In Fig. 6, his results for the shadow behind a single atom are compared to the present results for the shadow behind a string of atoms. The comparison is complicated by the

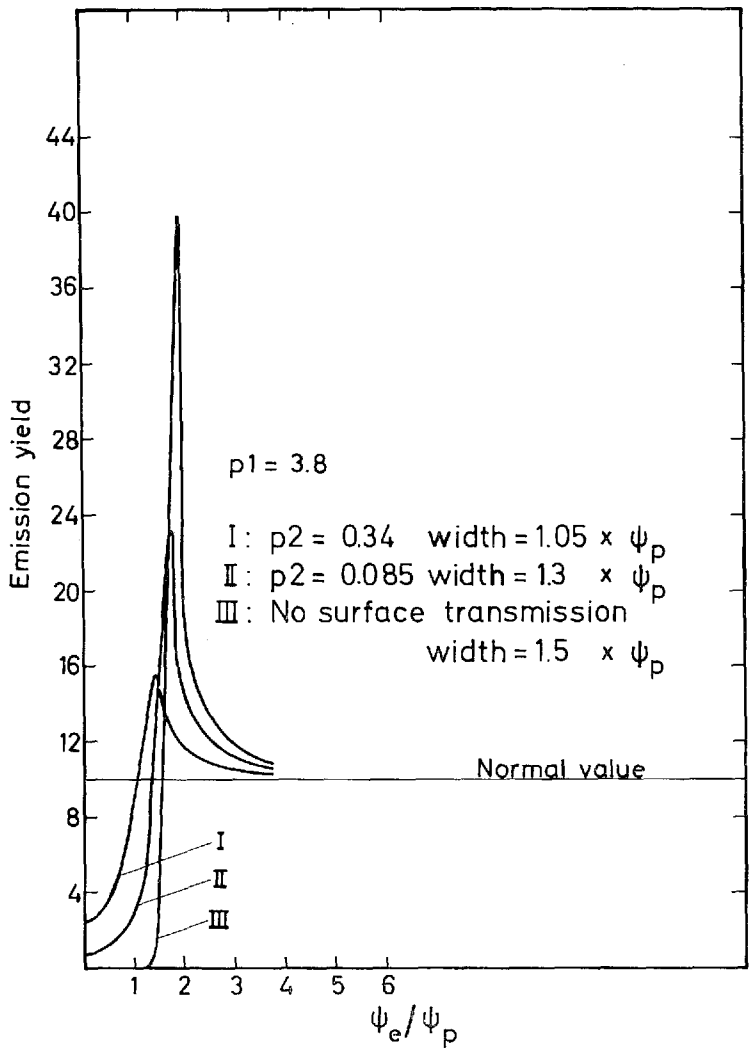

Fig. 8. Influence of the surface transmission on a planar dip illustrated by angular distribution of protons emitted from {110} plane in tungsten at room temperature. Actual value of $p2$ is 0.085.

difference of the potentials used in the two calculations (OEN uses an exponentially screened potential). The string calculation has therefore been repeated with an exponentially screened potential. The resulting curve is also shown in Fig. 6. It is seen that the width of the dip obtained with a Bohr potential is much smaller than that of the dip obtained with Lindhard's

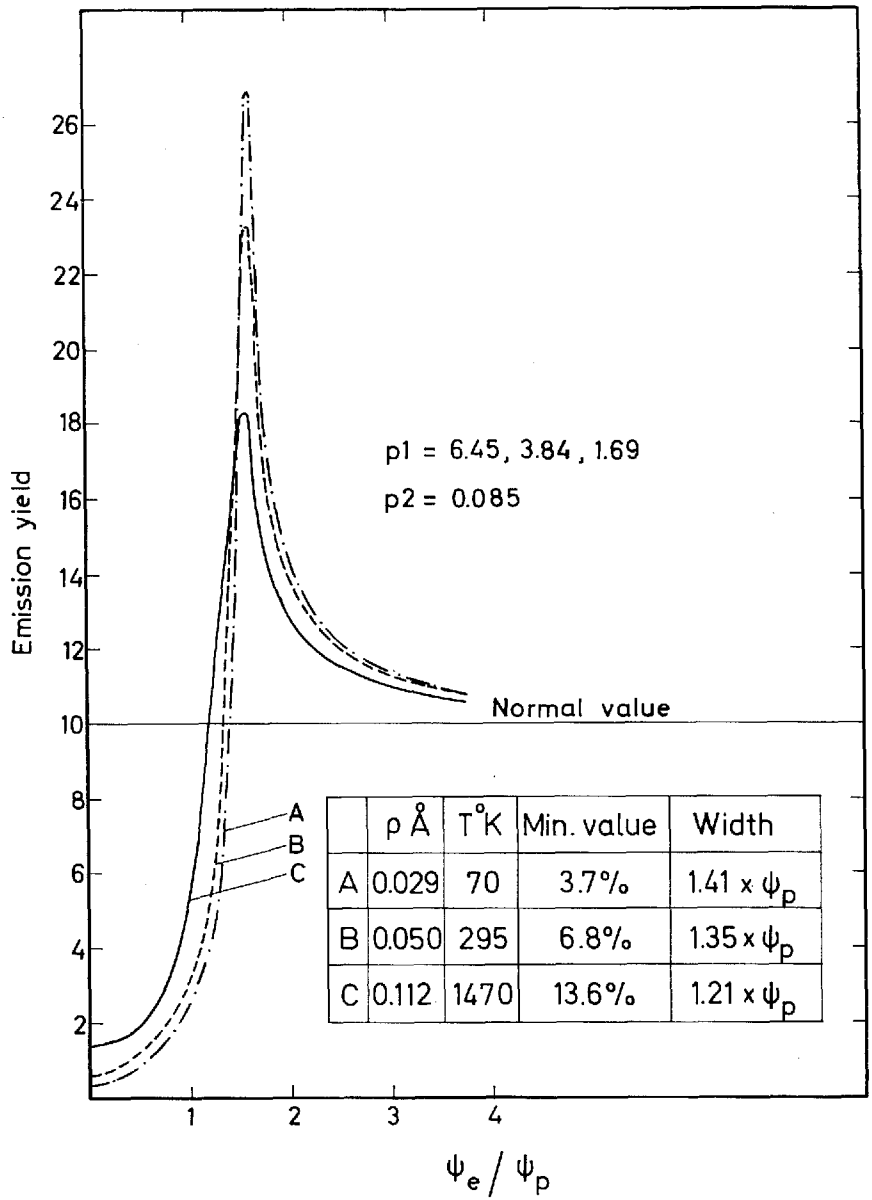

Fig. 9. Dependence on the vibrational amplitude ϱ of a {110} planar dip in tungsten.

standard potential. This is not surprising since in the actual case $\psi_1 \sim a/d$, i.e. scattering of the emitted particles at distances $\gtrsim a$ plays an important part, and in this region, the Bohr potential is known to decrease too rapidly.

The difference between curves II and III may be attributed to the scattering from the second, third, etc., neighbour on the string. As expected, the difference is largest for small angles.

Planar case

Two typical planar dips are shown in Fig. 7. We may compare the width at normal value with the respective values of ψ_p given by (25). This comparison is made in the figure. It is seen that ψ_p is a fairly good measure of the width.

Figure 8 illustrates the influence of the transmission through the surface and of the parameter $p2 = Ca/d$. It is seen that the influence of the transmission — as expected — is much larger than in the string case.

Figure 9 shows the dependence on ϱ of a planar dip. The planar dip shows a somewhat weaker ϱ-dependence than does the string dip. The minimum value is changing by a factor of 3.7 compared to a factor of 14.3 in Fig. 4. The width changes with a factor of 0.86 compared to a factor of 0.60 in Fig. 4.

§ 6. Discussion of Results

String case

Before comparing the results of the calculations with experiments, it may be appropriate to discuss briefly the kind of agreement to be expected. For this purpose, we may divide the string dip roughly into three regions:

1) The bottom of the dip
2) The side of the dip, i.e. the region where the yield rises rapidly to the normal value
3) The shoulder, i.e. the region just outside the dip where the dip is compensated by a yield higher than normal.

The main physical interest is concentrated on region 1), where the large dip in yield occurs. This dip may be characterized by the minimum yield $\chi_{\min}$. The value of $\chi_{\min}$ found in experiments depends critically on the experimental conditions. First of all, $\chi_{\min}$ is sensitive to all kinds of crystal defects, especially surface defects such as an oxide layer or even small deviations of the crystal structure near the surface from the bulk structure.

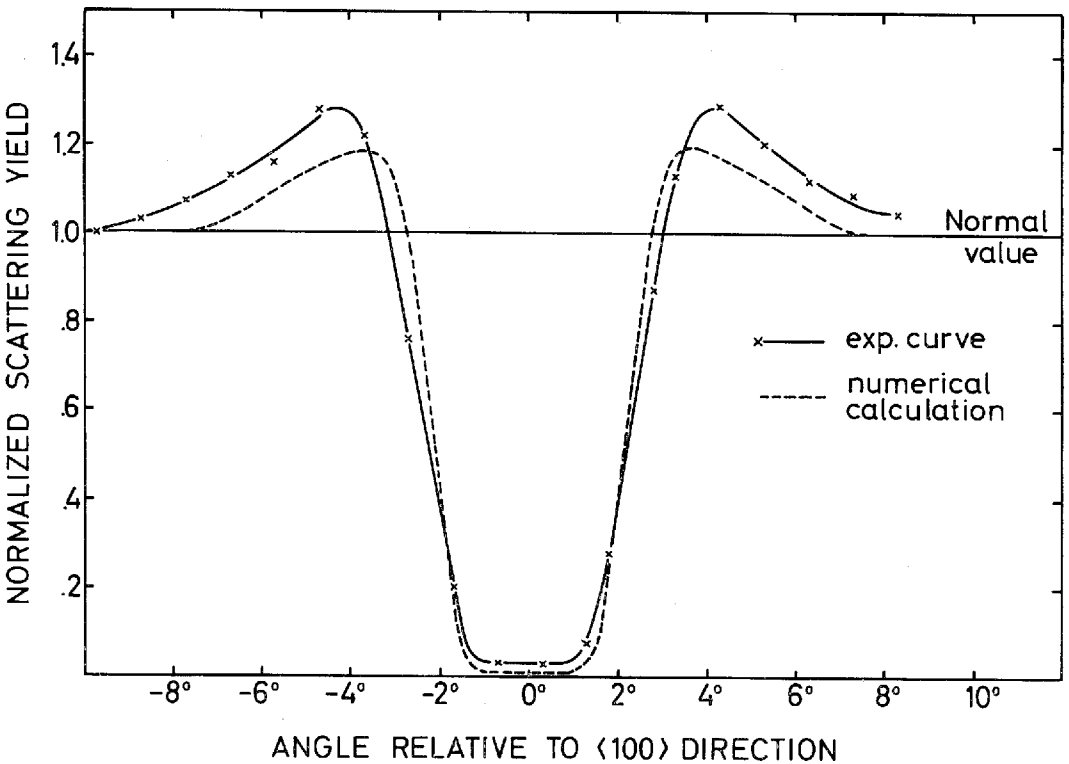

Fig. 10. Experimental[13] and calculated string dip in Rutherford scattering yield for 480 keV protons incident along a ⟨100⟩ direction on a tungsten crystal at 390° K.

Furthermore, under normal experimental conditions it is not possible to resolve the yield due to the first layer of the crystal from which the yield is normal. In most cases, some multiple scattering is also included in measurements of $\chi_{\min}$. A quantitative agreement between the numerically calculated value of $\chi_{\min}$ and the experimentally found value is therefore not to be expected. In favourable cases it has, however, been possible[10, 11] to measure $\chi_{\min}$ values of the same order as Lindhard's qualitative estimate, $\chi_{\min} = Nd\pi(\varrho^2 + a^2)$ (I, eq. (6.14))*.

Region 2) may be characterized by the width at half minimum of the dip. The width is not very sensitive to experimental conditions and should therefore show good agreement between calculation and experiment.

* In cases with very high depth resolution, more detailed information about the minimum yield and its variation with depth may be obtained as recently demonstrated by Bøgh[12]. For such cases, theoretical estimates considering the specific experimental conditions may be developed.

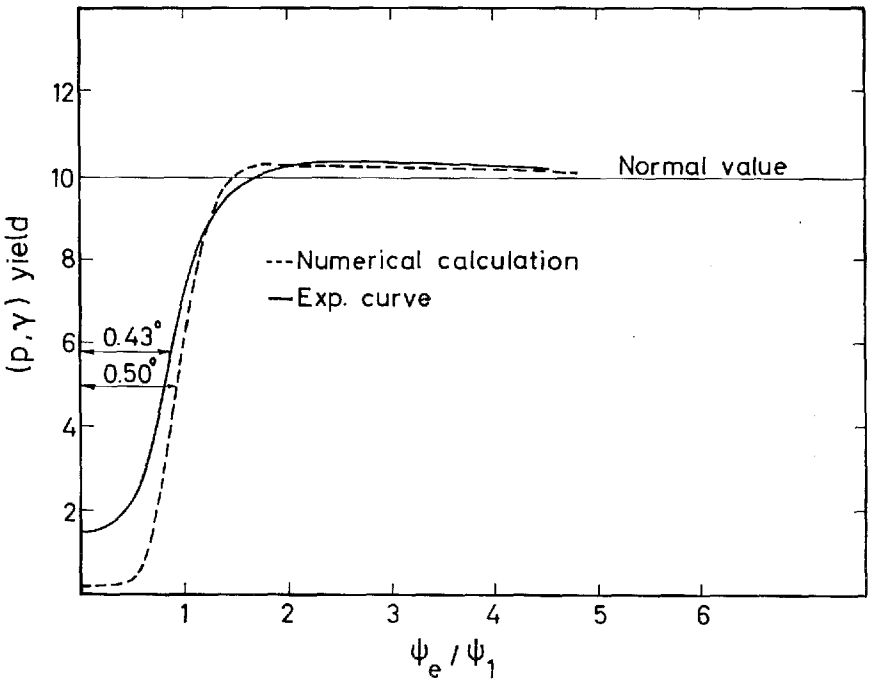

Fig. 11. Experimental[2] and numerically calculated string dip in (p,γ) yield for 1400 keV protons incident along a $\langle 110 \rangle$ direction on an aluminium crystal at room temperature.

Region 3) cannot be expected to show quantitative agreement, the main reason being that in most cases, the yield in this region is strongly influenced by planar effects. Clear experimental evidence of this influence is found in e.g. ref. 13). Measurements may, however, be expected to exhibit the qualitative features of the compensation mentioned in connection with Figs. 3 and 4.

Here, we shall not give a comprehensive comparison between the available experimental results and corresponding numerical calculations. A considerable amount of experimental results is found in refs. 11) and 13). In these references, the corresponding results of the numerical calculations are also given. To illustrate the kind of agreement found in most cases, two experimental and calculated string dips are compared in Figs. 10 and 11. As seen in these figures, the width of the experimental dip is well reproduced in the calculation.

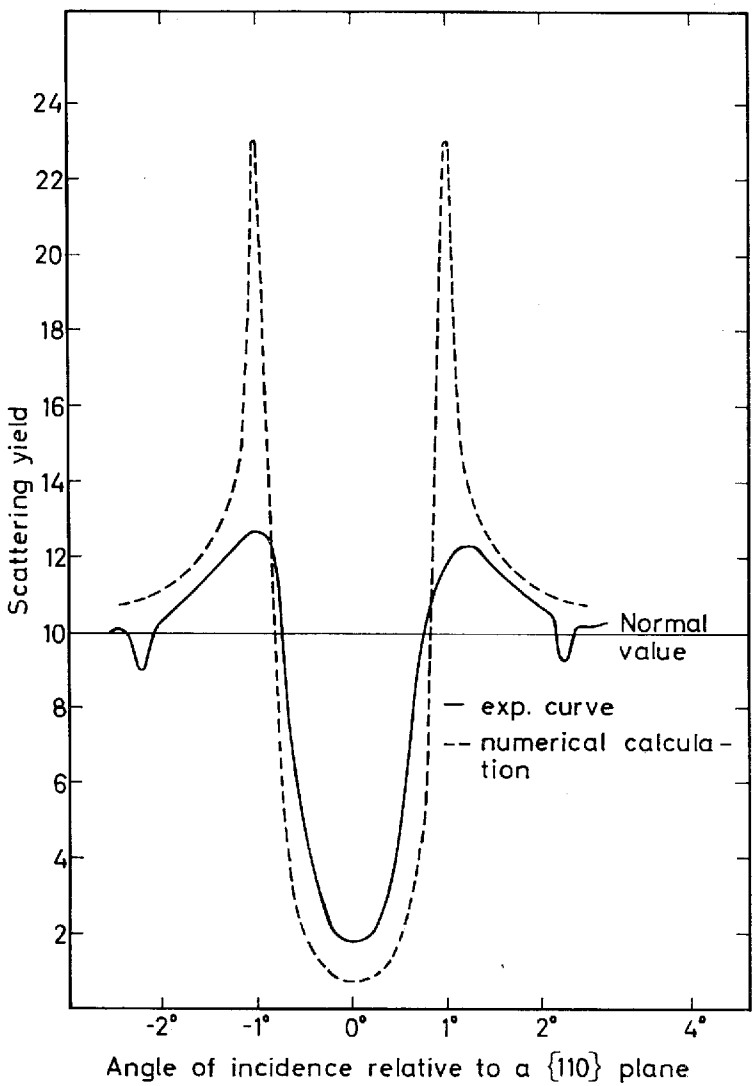

Fig. 12. Comparison between measured and calculated planar dip in Rutherford scattering yield for 480 keV protons incident along a {110} plane on a tungsten crystal at room temperature.

Planar case

The theoretical description of the planar case is not expected to be as accurate as the description of the string case and consequently, a less quantitative agreement is expected. The agreement obtained in the planar case is

illustrated in Fig. 12. The widths at normal value are in fair agreement but the minimum values differ by a factor of two, and the very high shoulder found in the calculation is not reproduced by experiment. This is not surprising since very little multiple scattering is required to smear out the extremely narrow shoulders.

Acknowledgements

The author is indebted to J. LINDHARD for stimulating interest and criticism, and also to J. A. DAVIES for numerous discussions. K. O. NIELSEN and P. JESPERSGAARD are thanked for a special effort to spur the writing of this paper.

Institute of Physics, University of Aarhus
Aarhus C, Denmark

References

1) E. Bøgh, J. A. Davies and K. O. Nielsen, Phys. Lett. **12**, 129 (1964).
2) J. U. Andersen, J. A. Davies, K. O. Nielsen and S. L. Andersen, Nucl. Instr. & Meth. **38**, 210 (1965).
3) E. Bøgh, Proceedings of the Cairo Solid State Conference, September 1966 (Plenum Press).
   L. Eriksson, J. A. Davies, J. Denhartog, H. J. Matzke and J. L. Whitton, Can. Nucl. Techn. **5**, no. 6 p. 40 (1966).
4) J. Lindhard, Mat. Fys. Medd. Dan. Vid. Selsk. **34**, no. 14 (1965).
5) P. Lervig, J. Lindhard and V. Nielsen, Nucl. Phys. A **96**, 481 (1967).
6) R. J. Glauber, Phys. Rev. **98**, 1692 (1955).
7) Internationale Tabellen zur Bestimmung von Kristallstrukturen **2**, 574 (1935).
8) R. S. Nelson, M. W. Thompson and H. Montgomery, Phil. Mag. **7**, 1385 (1962).
9) O. S. Oen, Phys. Lett. **19**, 358 (1965) and private communication.
10) E. Bøgh and E. Uggerhøj, Phys. Lett. **17**, 116 (1965) and Nucl. Instr. & Meth. **38**, 216 (1965).
11) J. A. Davies, J. Denhartog and J. L. Whitton, submitted to Phys. Rev.
12) E. Bøgh, Phys. Rev. Letters **19**, 61 (1967).
13) J. U. Andersen and E. Uggerhøj, to appear in Can. J. Phys. (1968).

Indleveret til Selskabet den 4. august 1967.
Færdig fra trykkeriet den 31. december 1967.